Singular Value Optimization in Inverse Electromagnetic Scattering

A. Capozzoli, *Member, IEEE*, C. Curcio, and A. Liseno

***Abstract*—We provide an approach to reformulate the problem of extracting the information on scatterers in inverse problems. The approach is based on the recently introduced concept of singular value optimization and exploits the single scattering hypothesis of the Born approximation. A two-dimensional geometry with multifrequency/single-view plane wave illumination and TM polarization with near-field acquisitions is considered. Numerical results show how it is possible to dramatically reduce the number of near-field samples against the canonical $\lambda_{\min}/2$ criterion.**

***Index Terms*—Born approximation, inverse scattering, multifrequency, sampling, singular value optimization (SVO).**

I. Introduction

THE applications of inverse electromagnetic scattering space in a wide range of disciplines requiring to noninvasively inspect an object under test [1]. Besides a purely optical area of interest [2], we mention as examples microwave imaging, including archaeological and civil applications and cultural heritages preservation [3], remote sensing [4], biomedical imaging [5], including magnetic resonance imaging [6] and computer aided tomography [7], nondestructive testing of materials [8], and geophysical prospection [9].

Common issue to inverse electromagnetic scattering as applied to the above-mentioned frameworks is extracting the maximum amount of information on the scatterer, when some *a priori* knowledge on the same is available [10].

Typically, field probes collect the information at different spatial positions. For this reason, we can formulate the problem as that of determining the minimum number of acquisition points and their "optimal" spatial distribution to reconstruct the scatterer "at the best" [10]. Sampling point number and positions will depend on the properties of the employed probes, on the shape and size of the acquisition domain, on the employed diversities (frequency, incidence angle) and on the *a priori* information on the scatterer, in terms of extent of the containing region and relative position to the measurement locations.

Recently, and with reference to the problem of reconstructing sources from their radiated fields, we have provided a new perspective to the field-sampling problem [10] based on a singular value optimization (SVO) approach. The technique relies on optimizing the singular values (SVs) behavior of the operator mapping the unknowns, i.e., the source, and the data, namely, the field samples. Such an approach has been extensively applied and validated in the case of near-field/far-field transformations in antenna characterization under different scanning geometries [11]–[13] and has proven significantly more convenient than the typical $\lambda/2$ criterion [13].

By regarding the scattered field as radiated by equivalent sources, then the idea underlying the approach in [10]–[13] can be fruitfully exploited to reformulate the problem of extracting the information in inverse scattering applications, provided that a linear mapping between scattered field and scatterers is established.

Purpose of this letter is then to give this new perspective to inverse scattering under the single scattering hypothesis. Attention is focused on a two-dimensional (2-D) geometry with multifrequency/single-view plane wave illumination, TM polarization, and near-field measurements. We deal with both the cases of transmission and reflection acquisitions. Features of the approach are as follows.

1) Exploits the Born approximation [1]: The link between scattered field and unknown permittivity turns to be linear.
2) By the SVO, a regularized solution is obtained [11]–[13]; in particular, the optimization selects the near-field sampling points (number and distribution) leading to the "best-conditioned" linear inversion problem [11]–[13].
3) Exploits weak *a priori* information on the scatterers in terms of: Extent of the region containing the objects and relative position between acquisition and investigation domains.

Under multifrequency illuminations, the canonical sampling step obeys the $\lambda_{\min}/2$ criterion [14], where $\lambda_{\min}$ is the minimum wavelength associated to the maximum employed frequency and the wavelength will be henceforth referred to the background medium. This criterion can lead to an exceedingly number of field samples. Here, we will show how our approach is capable to providing a set of "optimally" spaced points, unique for all the frequencies in the band, which dramatically reduces the number of samples as compared to the $\lambda_{\min}/2$ case.

II. Inverse Scattering Problem and the Inversion Approach

To illustrate the method and express the relevant operators, we assume that number and locations of the sampling points

Manuscript received September 25, 2016; accepted October 18, 2016. Date of publication December 21, 2016; date of current version May 1, 2017.

The authors are with the Dipartimento di Ingegneria Elettrica e delle Tecnologie dell'Informazione, Università di Napoli Federico II, I 80125 Naples, Italy (e-mail: a.capozzoli@unina.it; clcurcio@unina.it; liseno@unina.it).

Color versions of one or more of the figures in this letter are available online at http://ieeexplore.ieee.org.

Digital Object Identifier 10.1109/LAWP.2016.2622713

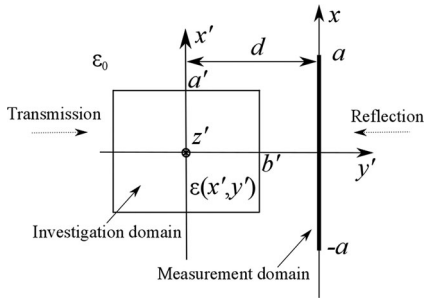

Fig. 1. Geometry of the problem.

have been already optimized, postponing the discussion on this point to the Section III.

Let us thus consider the 2-D geometry illustrated in Fig. 1, which involves cylindrical scatterers embedded in free space and with axis parallel to the y'-axis. The free-space permittivity is denoted by ε_0. The box $(-a', a') \times (-b', b')$ represents the region of interest, i.e., the box containing the scatterers wherein the permittivity distribution $\varepsilon(x', y')$ should be reconstructed. In other words, such a box represents part of the available *a priori* knowledge of the problem. The segment $(-a, a)$ of the x-axis represents the acquisition domain on which the scattered field is acquired and which is spaced a distance d apart from the x' -axis. The distance d will be assumed to be some $\lambda_{\max}$'s, where $\lambda_{\max}$ is the wavelength associated to the minimum frequency. The impinging field is assumed to be a TM-polarized plane wave traveling along the y'-axis and having varying frequency. We will assume to be able to arbitrarily fix the number and the values of the illuminating frequencies within a prescribed frequency band. We will also assume permittivity variations in $(-a', a') \times (-b', b')$, with the permeability spatially constant and equal to μ_0. According to Fig. 1, two cases are considered, namely, the case of reflection measurements, for which the plane wave propagates in the negative direction of the y'-axis, and that of transmission measurements, for which the plane wave propagates along the positive direction of the y'-axis.

Under the above hypotheses, the problem turns into a scalar one, and the only (z) component E_s of the scattered field can be written, apart from unessential constants, as

$$E_s(x,\beta) = \beta^2 \int_{-a'}^{a'} \int_{-b'}^{b'} H_0^{(2)}\left(\beta\sqrt{(x-x')^2+(d-y')^2}\right) \times E(x',y')\,\chi(x',y')\,dx'dy' \quad (1)$$

where β is the wavenumber in the background medium (void), $H_0^{(2)}(\cdot)$ is the Hankel function of zeroth order and second kind, E is the z-component of the total field within the region of interest, and $\chi(x', y') = (\varepsilon(x', y') - \varepsilon_0)/\varepsilon_0$ is the so-called contrast function, the unknown of the problem. In (1), $x \epsilon (-a, a)$ and $\beta \in (\beta_{\min}, \beta_{\max})$, where $\beta_{\min}$ and $\beta_{\max}$ correspond to the maximum and minimum employed frequencies, respectively.

Under the Born approximation and for unitary plane wave illumination, (1) becomes

$$E_s(x,\beta) = \beta^2 \int_{-a'}^{a'} \int_{-b'}^{b'} H_0^{(2)}\left(\beta\sqrt{(x-x')^2+(d-y')^2}\right) \times e^{-j\alpha\beta y'}\chi(x',y')\,dx'dy' \quad (2)$$

where $\alpha = -1$ or $\alpha = 1$ for reflection or transmission measurements, respectively. The relevant operators for such two cases are different, so the reconstruction capability of the approach for the two cases should be expected to be different.

Having the region of interest rectangular shape and discarding the scatterers' components contributing to the evanescent waves, the unknown contrast function χ is represented by the prolate spheroidal wave functions (PSWFs) [11]–[13] as [15], [16]

$$\chi(x',y') = \sum_{p=1}^{P}\sum_{q=1}^{Q} \alpha_{pq}\Phi_p[c_{x'}, x']\,\Phi_q[c_{z'}, y'] \quad (3)$$

where $\Phi_i[c_{w'}, w]$ is the ith 1-D PSWF with space-bandwidth product c_w [15], [16]; $c_{x'} = a'\beta_0$, $c_{y'} = b'\beta_0$, and β_0 is the average wavenumber in $(\beta_{\min}, \beta_{\max})$. In (3), $P = Int[4a'/\lambda_0]$ and $Q = Int[4b'/\lambda_0]$, where λ_0 is the wavelength corresponding to β_0. Unfortunately, there is no closed-form expression to the PSWFs. Their numerical calculation is a sensitive problem that must be carefully dealt with. A satisfactory solution has been devised in the literature by exploiting Legendre polynomial expansions see [17].

Furthermore, E_s is sampled at N, possibly unequally spaced, points $\{x_n\}_{n=1}^N$ and at M equally spaced wavenumbers β_m having sampling step $\Delta\beta$. In the present approach, to simplify the measurement configuration, the sampling points $\{x_n\}_{n=1}^N$ are unique for all the frequencies. As mentioned, N and $\{x_n\}_{n=1}^N$ are selected following an SVO. On the other side, the optimization of the wavenumbers β_m is particularly burdened, requires an appropriate processing, and is not a subject of this letter. The approach can be obviously extended to the case when the sampling locations change depending on the frequency, and the illumination frequencies are subject to optimization as well.

According to the above, (2) can be rewritten in a matrix form as

$$\underline{E}_s = \underline{\underline{T}}\,\underline{\alpha} \quad (4)$$

where $\underline{E}_s$ is the vector containing the $N \times M$ field samples $E_s(x_n, \beta_m)$, $\underline{\alpha}$ is the vector containing the expansion coefficients α_{pq}, and the matrix $\underline{\underline{T}}$ has entries

$$\beta^2 \int_{-a'}^{a'} \int_{-b'}^{b'} H_0^{(2)}\left(\beta\sqrt{(x_n-x')^2+(d-y')^2}\right) e^{-j\alpha\beta y'} \Phi_p[c_{x'}, x']\,\Phi_q[c_{z'}, y']\,dx'dy'. \quad (5)$$

The problem amounts to the determination of χ in terms of the α_{pq}'s, starting from $E_s(x_n, \beta_m)$. Unfortunately, the inversion of (4) is affected by the ill-conditioning of $\underline{\underline{T}}$, so that a regularized approach should be exploited. A possible solution is provided by the truncated SVD (TSVD) approach [11], even if other regularization strategies are possible [18]. Here, we propose the SVO

having the twofold advantage of providing regularization and furnishing the number and locations of the "optimal" samples.

III. Choice of Number and Locations of Near-Field Samples

We turn to consider the problem of selecting "the most convenient" N and $\{x_n\}_{n=1}^{N}$.

We first underline that, for a fixed choice of the representation of the contrast function [see (4)], the matrix $\underline{\underline{T}}$ is not univocally defined since it depends on the selection of both N and $\{x_n\}_{n=1}^{N}$. Accordingly, a family of matrices $\underline{\underline{T}}$ is available, with different behaviors of the SVs depending on N and on $\{x_n\}_{n=1}^{N}$. Having at disposal this degree of freedom, it is then desirable to perform the inversion using the element of the family with "the most convenient" singular value behavior, i.e., that corresponding to the "best possible conditioning." To be more precise, among all the possible matrices $\underline{\underline{T}}$ and for a fixed N, it is convenient to choose $\{x_n\}_{n=1}^{N}$ providing the "flattest" singular value behavior.

We also recall that, throughout the literature, the Shannon number

$$\Phi\left(N, x_1, x_2, \ldots, x_N\right) = \sum_{k=1}^{K} \frac{\sigma_k}{\sigma_1} \tag{6}$$

where $K = \min\{NM, PQ\}$, which is the "area" subtended by the normalized SVs σ_k/σ_1 being ordered in a decreasing way, is considered as a measure of the information that can be extracted from the data to retrieve the unknown [10]. Accordingly, the samples (number and positions) on $(-a, a)$ should be selected to maximize Φ. Obviously, it is expected that, for a fixed N, the maximization of Φ providing $\{x_n\}_{n=1}^{N}$ and leading to the $\Phi_{\mathrm{opt}}(N)$ value, returns the most convenient samples distribution to collect, with just N probings, the information carried by the scattered field on the observation domain. However, by increasing N, it is expected that $\Phi_{\mathrm{opt}}(N)$ increases, but not indefinitely: Too many points too close each other are not able to provide independent information [19]. Accordingly, $\Phi_{\mathrm{opt}}(N)$ as a function of N must exhibit a horizontal asymptote. The number N at the saturation knee represents then the minimum number of samples needed to achieve all the information available on $\underline{\alpha}$ from the domain $(-a, a) \times (\beta_{\min}, \beta_{\max})$.

We finally mention that, to favor a successful optimization process, the sampling locations are represented with a low number of parameters by a properly defined "mapping function." For further details, see [10]–[13].

The SVO thus provides a regularization to the problem consisting first in selecting the best conditioned discrete version of the relevant operator against the free parameters (number and position of the field samples, in our case) and then in controlling the residual degree of ill-conditioning by traditional techniques.

IV. Numerical Results

As numerical test cases, we consider $a' = 2\lambda_0, b' = 2\lambda_0, a = 56\lambda_0$, and $d = 32\lambda_0$, where λ_0 is the wavelength corresponding to the center frequency. We also suppose that $\frac{\lambda_{\max}}{\lambda_0} = 0.8$ and $\frac{\lambda_{\min}}{\lambda_0} = 0.5$, where $\lambda_{\max}$ and $\lambda_{\min}$ are the wavelengths at the lowest and highest employed frequencies, respectively. A number of 15 uniformly spaced frequencies have been exploited, and 15×15 PSWFs, corresponding to the "visible" PSWFs [10]–[13], have been employed to expand the unknown contrast function.

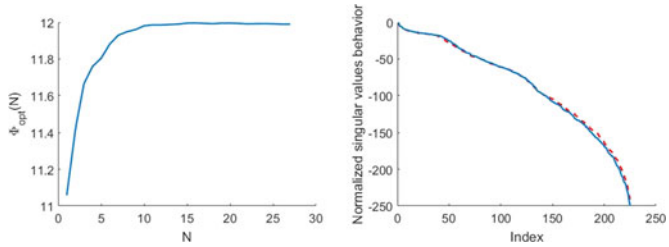

Fig. 2. Reflection test case. Left: $\Phi_{\mathrm{opt}}(N)$ curve for the selection of N. Right: Singular value behavior for the canonical (dashed) and "optimized" (solid) samplings.

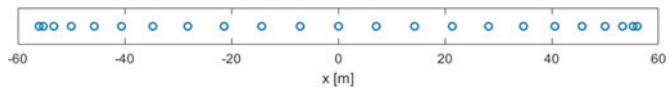

Fig. 3. Reflection test case. "Optimal" location of the sampling points.

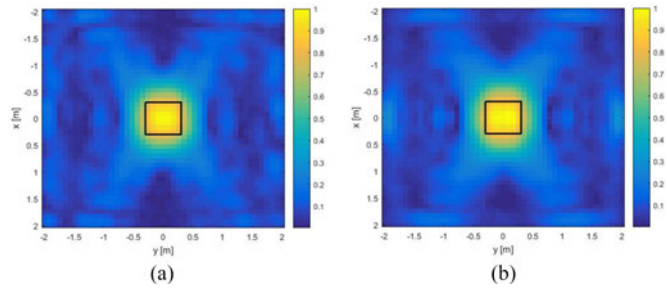

Fig. 4. (a) Reflection case: Reconstruction with canonical sampling. (b) Reflection case: Reconstruction with "optimized sampling."

Let us consider first the case of reflection measurements. The behavior of $\Phi_{opt}(N)$ is depicted in Fig. 2 (left), from which it is seen that the curve is well saturated approximately for $N = 23$.

Accordingly, we will consider a number of 23 sampling points, whereas we notice that the $\lambda_{\min}/2$ criterion would lead to a significantly larger number of 420 sampling locations. The optimized sampling points are displayed in Fig. 3. Fig. 2 (right) depicts the SVs behavior of matrix $\underline{\underline{T}}$ in (4) for the two cases of "optimized sampling" and canonical $\lambda_{\min}/2$ sampling. As it can be seen, the same behavior, and thus the degree of ill-conditioning, is obtained with a significantly lower number of measurements. Finally, we show the reconstruction capabilities of the approach. To this end, we have considered a homogeneous scatterer of size 0.6×0.6 m. Fig. 4(a) and (b) shows the reconstructions achieved by TSVD when canonical uniform sampling with 420 sampling locations and "optimized," nonuniform sampling with 23 sampling locations are considered, respectively. The data have been corrupted with additive Gaussian noise with signal-to-noise ratio of 30 dB, and the SVs have been filtered using a threshold set 30 dB below the maximum one.

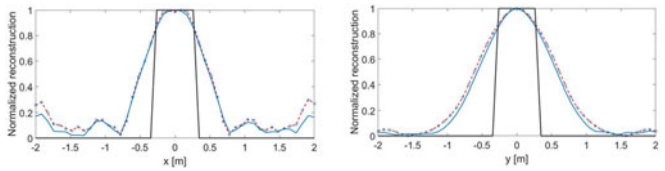

Fig. 5. Reflection test case: Comparison between the reconstructions with canonical sampling (dashed red line), "optimized sampling" (solid blue line) and reference object (solid black line). Stars represent canonical sampling in the noiseless case. *Left*: cut along the *x*-axis. *Right*: cut along the *y*-axis.

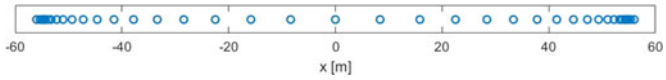

Fig. 6. Transmission case. "Optimal" location of the sampling points.

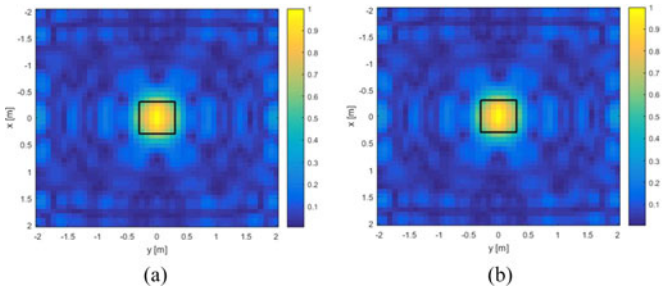

Fig. 7. (a) Transmission case: Reconstruction with canonical sampling. (b) Transmission case: Reconstruction with "optimized sampling."

As it can be expected and appreciated from Fig. 4(a) and (b), the reconstruction quality following the proposed "optimized sampling" is the same as that for the canonical sampling, but it is achieved with a significantly lower number of measurements. This can be better appreciated from Fig. 5, where the comparison is performed showing cuts along coordinate axes. As a consequence, uniform sampling with the $\lambda_{\min}/2$ is redundant.

Let us consider transmission measurements. In this case, the "optimal" number of sampling points has been $N = 50$. The SVs behavior is not reported for the sake of brevity, but their relative behavior is totally analogous to that of the previous case. The "optimized" sampling points are displayed in Fig. 6. Again, for transmission measurements, a significantly lower number of sampling locations is obtained when using the SVO as compared to the 420 sampling locations of the $\lambda_{\min}/2$ criterion. Finally, Fig. 7(a) and (b) shows the reconstructions achieved by the TSVD when canonical uniform sampling with 420 sampling locations and "optimized," nonuniform sampling with 50 sampling locations are considered, respectively.

Once again, the data have been corrupted with noise as before, and the SVs have been filtered using the same threshold. As it can be expected and appreciated from Fig. 7(a) and (b), the reconstruction quality following the proposed "optimized sampling" is the same as that for the canonical one, but it is achieved with a significantly lower number of measurements.

REFERENCES

[1] A. J. Devaney, *Mathematical Foundations of Imaging, Tomography and Wavefield Inversion*. New York, NY, USA: Cambridge Univ. Press, 2012.
[2] T. S. Ralston, D. L. Marks, P. S. Carney, and S. A. Boppart, "Inverse scattering for optical coherence tomography," *J. Opt. Soc. Amer. A*, vol. 23, no. 5, pp. 1027–1037, 2006.
[3] N. Linford, P. Linford, and L. M. A. Payne, "Stepped frequency ground-penetrating radar survey with a multi-element array antenna: Results from field application on archaeological sites," *Archaeol. Prospection*, vol. 17, no. 3, pp. 187–198, Jul.–Sep. 2010.
[4] A. Capozzoli, C. Curcio, and A. Liseno, "Fast GPU-based interpolation for SAR backprojection," *Prog. Electromagn. Res.*, vol. 133, pp. 259–283, 2013.
[5] T. M. Grzegorczyk, P. M. Meaney, P. A. Kaufman, R. M. diFlorio-Alexander, and K. D. Paulsen, "Fast 3-D tomographic microwave imaging for breast cancer detection," *IEEE Trans. Med. Imag.*, vol. 31, no. 8, pp. 1584–1592, Aug. 2012.
[6] J. A. Fessler, "Model-based image reconstruction for MRI," *IEEE Signal Process. Mag.*, vol. 27, no. 4, pp. 81–89, Jul. 2010.
[7] M. B. Nagarajan, P. Coan, M. B. Huber, P. C. Diemoz, C. Glaser, and A. Wismüller, "Computer-aided diagnosis in phase contrast imaging X-ray computed tomography for quantitative characterization of ex vivo human patellar cartilage," *IEEE Trans. Biomed. Eng.*, vol. 60, no. 10, pp. 2896–2903, Oct. 2013.
[8] M. Jamil, M. K. Hassan, H. M. A. Al-Mattarneh, and M. F. M. Zain, "Concrete dielectric properties investigation using microwave nondestructive techniques," *Mater. Struct.*, vol. 46, no. 1, pp. 77–87, Jan. 2013.
[9] D. G. Drogoudis, G. A. Kyriacou, and J. N. Sahalos, "Microwave tomography employing an adjoint network based sensitivity matrix," *Prog. Electromagn. Res.*, vol. 94, pp. 213–242, 2009.
[10] A. Capozzoli, C. Curcio, A. Liseno, and P. Vinetti, "Field sampling and field reconstruction: A new perspective," *Radio Sci.*, vol. 45, 2010, Art. no. RS6004, doi:10.1029/2009RS004298.
[11] A. Capozzoli *et al.*, "Dielectric field probes for very-near-field and compact-near-field antenna characterization," *IEEE Antennas Propag. Mag.*, vol. 51, no. 5, pp. 118–125, Oct. 2009.
[12] A. Capozzoli *et al.*, "Photonic probes and advanced (also phaseless) near-field far-field techniques," *IEEE Antennas Propag. Mag.*, vol. 52, no. 5, pp. 232–241, Oct. 2010.
[13] A. Capozzoli, C. Curcio, G. D'Elia, and A. Liseno, "Singular value optimization in plane-polar near-field antenna characterization," *IEEE Antennas Propag. Mag.*, vol. 52, no. 2, pp. 103–112, Apr. 2010.
[14] H. J. Shin, R. M. Narayanan, and M. Rangaswamy, "Diffraction tomography for ultra-wideband noise radar and imaging quality measure of a cylindrical perfectly conducting object," in *Proc. IEEE Radar Conf.*, Cincinnati, OH, USA, May 19–23, 2014, pp. 702–707.
[15] H. J. Landau and H. O. Pollak, "Prolate spheroidal wave functions, Fourier analysis and uncertainty—III: The dimension of essentially time- and band-limited signals," *Bell Syst. Tech. J.*, vol. 41, pp. 1295–1336, Jul. 1962.
[16] B. R. Frieden and E. Wolf, "Evaluation, design and extrapolation methods for optical signals, based on use of the prolate functions," *Prog. Opt.*, vol. 9, pp. 311–407, 1971.
[17] H. Xiao, V. Rokhlin, and N. Yarvin, "Prolate spheroidal wavefunctions, quadrature and interpolation," *Inverse Probl.*, vol. 17, no. 4, pp. 805–838, Aug. 2001.
[18] A. Kirsch, *An Introduction to the Mathematical Theory of Inverse Problems*, Bristol, NY, USA: Springer-Verlag, 1996.
[19] R. Piestun and D. A. B. Miller, "Electromagnetic degrees of freedom of an optical system," *J. Opt. Soc. Amer. A*, vol. 17, no. 5, pp. 892–902, May 2001.